Cellular Signalling 63 (2019) 109385

Contents lists available at ScienceDirect

Cellular Signalling

journal homepage: www.elsevier.com/locate/cellsig

Drug-resistant endothelial cells facilitate progression, EMT and chemoresistance in nasopharyngeal carcinoma via exosomes

Limin Huang[a,*,1], Chaoquan Hu[b,**,1], Hui Chao[a], Yu Zhang[a], Yong Li[a], Jing Hou[a], Zhong Xu[a], He Lu[c], Hong Li[c], Hui Chen[a,*]

[a] Department of Oncology, Guizhou Provincial People's Hospital, Guizhou Cancer Center, Guiyang, Guizhou, China
[b] Department of Surgery, Affiliated Hospital, GuiZhou Medical University, Guiyang 550004, China
[c] INSERM UMR_S 1165/Paris 7, Hôpital Saint Louis, Paris, France

ARTICLE INFO

Keywords:
Nasopharyngeal carcinoma
Drug resistance
Human microvascular endothelial cells (HMECs)
Exosome

ABSTRACT

Recent antitumor drug development has included investigation of a wide variety of anti-angiogenesis therapies. Because cancer cells in tumors require new blood vessels to grow and spread, they stimulate capillary proliferation from existing vessels as well as new vessel formation from endothelial precursor cells. Our previous findings suggested that drug resistance in mouse endothelial cells supported tumor growth, but the relationship between endothelial cells (ECs) and nasopharyngeal carcinoma (NPC) cells remained unclear. Exosomes are small membrane vesicles that are released by several cell types, including human microvascular ECs (HMECs). Exosomes carrying membrane and cytoplasmic constituents have been described as participants in a novel mechanism of cell-to-cell communication. In the present study, we investigated the mechanisms underlying the interactions between HMECs and NPC cells. We found that drug-resistant HMECs secreted small heterogeneous 40–100 nm vesicles, defined as exosomes. Co-incubation of NPC cells with doxorubicin-resistant (R-DOX) HMEC-derived exosomes resulted in promotion of their proliferation, migration, and chemoresistance, as well as changes in the expression of epithelial–mesenchymal transition (EMT) markers. These effects were significantly inhibited by treatment with GW4869 (an exosome inhibitor). We also found that GW4869 inhibited the stimulation of drug-resistant HMECs on NPC progression by modulating EMT in vivo. These data suggest that exosomes participate in a novel mechanism by which drug-resistant ECs enhance NPC progression.

1. Introduction

Nasopharyngeal cancer (NPC) is characterized by an extremely skewed geographical distribution [1]. Over 80% of cases worldwide occur in Asia. Of this total, in 2012, China comprised the largest percentage (38%), followed by Indonesia (15%), Vietnam (6%), and India (4%). NPC is comparatively rare in North America and Europe. In 2014, NPC affected 7.9 per 100,000 population in Hong Kong, compared with < 1.0 per 100,000 population in North America and Europe [2].

Despite advances in diagnostic and therapeutic modalities, NPC remains a highly malignant and lethal disease. The complications of NPC are compounded by the anatomical proximity of physiological structures. The therapy of choice has been radiotherapy. Chemotherapy is used in patients that have advanced loco-regional disease, although a standard chemotherapeutic regimen for NPC has not as yet been established [3]. Drug treatment has been shown to improve overall survival [4]. Surgery is reserved for palliation of recurrent disease.

Resistance to chemotherapeutic agents is a recurring theme throughout tumor biology. Efforts to design agents to overcome chemoresistance (or conversely to enhance chemosensitivity) are ongoing, and this is true for NPC [3,5].

In recent years, exosomes have become an area of interest in oncology for various types of cancer, including NPC [6]. Exosomes have been associated with the development of chemoresistance in a variety of cancers [7–11]. Exosomes derived from vascular epithelial cells have been implicated in the conferral of chemoresistance and metastatic potential; however, the role of exosomes derived from vascular endothelial cells in progression and chemoresistance in NPC remains

* Correspondence to: L. Huang, H. Chen, Department of Oncology, Guizhou Provincial People's Hospital, Guizhou Cancer Center, 83 Zhongshan East Rd, Guiyang, Guizhou 550003, China.
** Correspondence to: C. Hu, Department of Surgery, Affiliated Hospital, GuiZhou Medical University, 550004 Guiyang, China.
E-mail addresses: liminhuang7610@outlook.com (L. Huang), kevinhucn@yahoo.com (C. Hu), 1728436708@qq.com (H. Chen).
[1] Limin Huang and Chaoquan Hu contributed equally to this work.

https://doi.org/10.1016/j.cellsig.2019.109385
Received 9 May 2019; Received in revised form 29 July 2019; Accepted 3 August 2019
Available online 05 August 2019

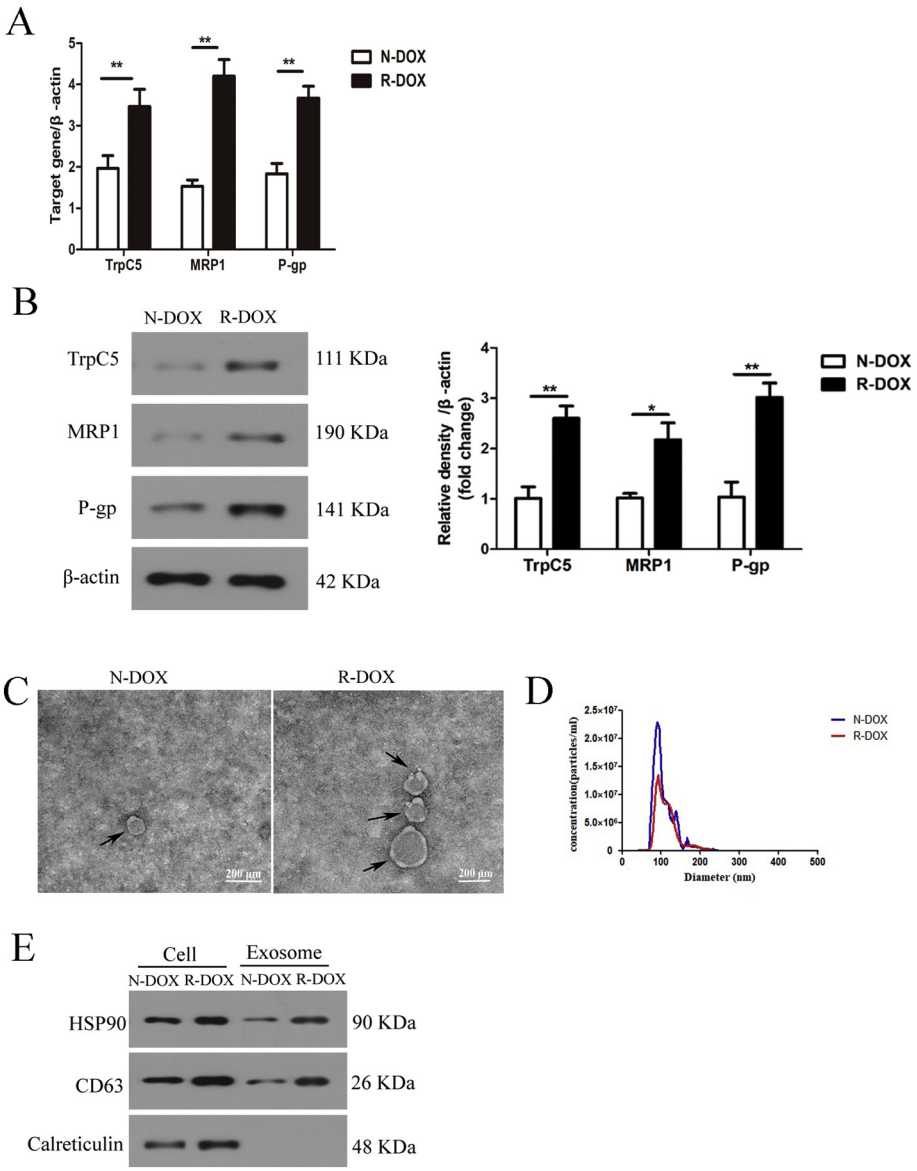

Fig. 1. Establishment of drug-resistant HMECs and characterization of the derived exosomes. (A,B) Real time PCR and western blot analysis of TrPC5, MRP1, and P-gp levels in drug-resistant HMECs (R-DOX) and non-resistant cell lines (N-DOX). The data used to determine the ratio were obtained from three repeated blots. *: $P < .05$, **: $P < .01$ in comparison with the controls. (C,D) Transmission electron microscopy and NTA of exosomes derived from drug-resistant and non-resistant HMECs indicated that more exosomes were secreted from drug-resistant endothelial cells. The scale bars indicate 200 nm, and the arrows indicate typical exosomes. (E) Exosomal positive markers Hsp90 and CD63 were detected in naive, R-DOX HMEC-derived, and N-DOX HMEC-derived exosomes by western blotting, whereas the negative marker calreticulin was not detected.

unknown. Therefore, we investigated the relationship between human microvascular endothelial cells (HMECs) and NPC, as well as the question as to whether exosomes derived from HMECs may play a role in progression and metastasis in NPC.

2. Results

2.1. Establishment of drug-resistant HMECs and characterization of exosomes

First, we tested whether drug-resistant HMECs expressed chemoresistance markers. The genes encoding TrPC5, MRP1, and P-gp were associated with drug resistance. We therefore measured the mRNA and protein levels of TrPC5, MRP1, and P-gp in both drug-resistant and non-drug-resistant HMECs. We found that TrPC5, MRP1, and P-gp were significantly more highly expressed in drug-resistant HMECs than in non-drug-resistant cells (Fig. 1A, B). Next, we used transmission electron microscopy of ultracentrifugation products to evaluate the levels of exosome production by each cell type and the size distribution of the isolated particles was measured by nanoparticle tracking analysis (NTA). We found that an equal number of drug-resistant HMECs produced substantially greater numbers of exosomes per field than control cells, that were of the appropriate size (40–100 nm) (Fig. 1C). NTA indicated that doxorubicin-non-resistant exosomes (N-DOX Exo) and doxorubicin-resistant exosomes (R-DOX Exo) were predominantly ~100 nm in size, and the concentrations of the 100 nm particles were calculated to be 1.2×10^7 particles/ml and 2.3×10^7 particles/ml, respectively (Fig. 1D). We then measured the levels of exosome markers Hsp90 [12] and CD63 in HMEC-derived exosomes from naïve drug-resistant and non-drug-resistant cells. We found that both Hsp90 and CD63 expression was substantially greater in drug-resistant-derived exosomes than in non-drug-resistant-derived exosomes (Fig. 1E). These data suggested that we had successfully established drug-resistant HMECs and that these cells produced substantial amounts of exosomes.

2.2. Drug-resistant HMECs promoted the expression of oncogenic phenotypes in NPC cells

We next determined whether exposure of NPC cells to drug-resistant HMECs would affect the expression of oncogenic phenotypes in NPC cells. Using a CCK-8 assay, we found that exposure to drug-resistant HMECs for 24, 48, 72, and 96 h increased cell viability in both NPC lines (5-8F and HONE1); non-resistant HMECs and control cells showed no significant effect (Fig. 2A, B). We next examined the effect of HMEC

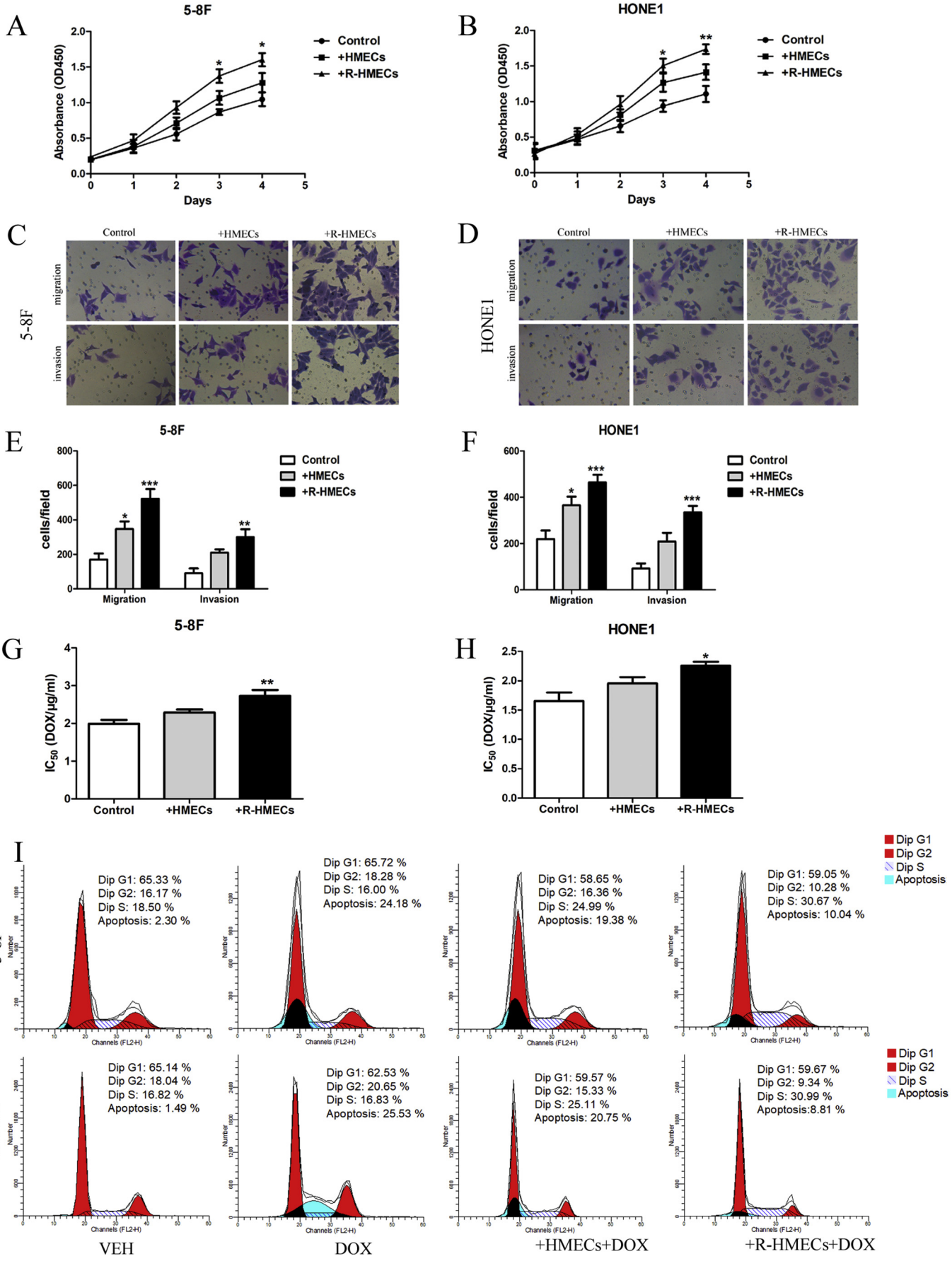

(caption on next page)

Fig. 2. Drug-resistant HMECs enhance the oncogenic phenotype of NPC cells. 5-8F (A) and HONE1 (B) cells in serum-free media were incubated with the indicated amounts of drug-resistant and non-resistant HMECs for 24, 48, 72, and 96 h, and cell viability was measured using a CCK-8 assay. (C&D) Cell migration and invasion properties as determined by a Transwell assay and crystal violet staining. (E&F) Statistical results for (C&D). Inhibitory concentration to produce 50% cell death of 5-8F (G) and HONE1 (H) cells incubated with drug-resistant HMECs was higher than that of NPCs with non-resistant HMECs. (I) Effects of DOX on 5-8F and HONE1 cell cycle distribution and the apoptosis rate. Cells were incubated with or without drug-resistant and non-resistant HMECs for 48 h. The data are presented as the means ± SEM of three independent experiments. $^{*}P < .05$ $^{**}P < .01$. (For interpretation of the references to colour in this figure legend, the reader is referred to the web version of this article.)

exposure on the cell migration and invasion properties of NPC cells. Using Transwell assays, we found that both the migration and invasion capabilities of NPC cell lines were significantly greater after exposure to drug-resistant HMECs than to non-drug-resistant HMECs (Fig. 2C–F).

We next examined whether exposure to resistant HMECs conferred doxorubicin resistance to NPC cell lines. We found that exposure to drug-resistant HMECs significantly increased the 50% lethal dose (LD_{50}) of doxorubicin in both 5-8F and HONE1 cells (Fig. 2G, H).

To examine the effects of exposure to drug-resistant HMECs on NPC cell cycle distribution and apoptosis rates, we incubated 5-8F and HONE1 cells with or without resistant and non-resistant HMECs for 48 h. We found that the numbers of apoptotic cells were significantly greater in NPCs treated with the non-resistant HMECs. Taken together, these data suggest that co-culture with drug-resistant HMECs promoted the expression of oncogenic phenotypes in NPC cells.

2.3. Drug-resistant HMECs acted on NPC cells by delivering exosomes

GW4869 is an inhibitor that can block exosome secretion. First, we determined whether GW4869 could successfully block exosome secretion in drug-resistant HMECs. Vesicles were found to be predominantly ~100 nm in size, and the concentrations of 100-nm vesicles were found to be 2.2×10^7 particles/ml and 1.0×10^7 particles/ml from resistant (*R*)-HMECs and R-HMECs + GW4869, respectively, as determined by NTA (Fig. 3A). Furthermore, GW4869 significantly inhibited the expression of exosome markers HSP90 and CD63, as determined by western blot analysis (Fig. 3B). Next, we explored the role of R-DOX HMEC-derived exosomes in the oncogenic effects of NPC cells. We performed Transwell migration and invasion assays and found that exosome inhibitor GW4869 significantly inhibited the migration and invasion of 5-8F and HONE1 cells that had been exposed to R-DOX HMEC-derived exosomes (Fig. 3C–H). We then measured the effects of doxorubicin on the cell cycle distributions and apoptosis rates of NPC cells that had been treated with exosomes derived from drug-resistant HMECs, treated with or without GW4869, for 48 h. We found that GW4869 exposure led to substantially fewer NPC cells in S-phase and substantially greater numbers of NPC cells undergoing apoptosis (Fig. 3I). These results demonstrated that R-DOX HMEC-derived exosomes suppress G2/M arrest in both 5-8F and HONE1 cells to confer drug resistance to other cancer cells.

2.4. Nasopharyngeal carcinoma (NPC) cells underwent epithelial–mesenchymal transition (EMT) mediated by exosomes released from HMECs

We next looked at the effect of R-DOX HMEC-derived exosomes on the expression of EMT markers in NPC cells. We incubated NPC cells with exosomes from drug-resistant or non-drug-resistant HMECs treated with or without GW4869 and performed immunofluorescence staining for E-cadherin (an epithelial marker) and vimentin (a mesenchymal marker). We found that R-DOX HMEC-derived exosomes substantially decreased staining for E-cadherin and increased staining for vimentin. Both effects were substantially blunted by pre-treatment with GW4869 (Fig. 4A, B).

We confirmed these results using western blotting. Exposure to R-DOX HMEC-derived exosomes substantially decreased protein expression of E-cadherin and increased expression of vimentin by NPC cells in a manner that was blunted by GW4869 (Fig. 4C–F). Using western blotting, we found that expression levels of chemoresistance markers MRP1 and P-gp were greater in NPC cells exposed to R-DOX HMEC-derived exosomes than in control cells and that this effect was blunted by GW4869 (Fig. 4C–F). Taken together, these data suggest that co-incubation with R-DOX HMEC-derived exosomes promoted EMT in NPC cells.

2.5. Drug-resistant HMECs promoted NPC xenograft growth in nude mice via exosomes

Finally, we examined the effects of drug-resistant HMECs on NPC tumor activity using a nude mouse xenograft model. We inoculated nude mice with 5-8F cells with or without drug-resistant HMECs. The mice were treated with or without doxorubicin and/or GW4869 for 27 days. We then measured tumor weights and volumes and performed histochemistry. We found that co-injection of drug-resistant HMECs was associated with significantly greater tumor weights and volumes. Doxorubicin injections diminished this effect and co-injection with GW4869 had an even greater effect on diminishing tumor growth (Fig. 5A–C).

We also employed the nude mouse model to examine the effects of drug-resistant HMECs on NPC lung metastasis using a live imaging analysis. Co-injection of drug-resistant HMECs greatly enhanced the extent of lung metastasis. Treatment with doxorubicin blunted this effect, and the combination of doxorubicin and GW4869 reduced metastases to control levels (Fig. 5D, E).

From mice in the tumor-growth model (Fig. 5A–C), we subjected tumors to immunohistochemical and TUNEL staining. We found that mice co-injected with drug-resistant HMECs had significantly greater expression levels of chemoresistance marker MRP1, mesenchymal marker vimentin, proliferation marker Ki67, and apoptosis marker TUNEL staining. Doxorubicin treatment significantly inhibited the effect of drug-resistant HMECs and the addition of GW4869 returned these expression levels to baseline (Fig. 5F, G). Taken together, these data suggest that drug-resistant HMECs promote tumor growth and drug resistance in vivo via an exosome-mediated pathway.

3. Discussion

All cancers are characterized, at least in part, by uncontrolled growth and division of cancer cells. Indeed, early cancer research efforts and therapeutics focused on the mechanisms of the cell cycle, particularly cell division, and ways to disrupt this [13]. However, in recent years, additional features have revealed themselves as important, and sometimes essential, for cancer cell proliferation and metastasis. These features include, for carcinomas, the process of EMT. For solid tumors, angiogenesis has become increasingly recognized as an important feature. Finally, resistance to therapeutic modalities, particularly chemoresistance, has become an area of intense research.

In the present study, we explored a mechanism that involves all of these phenomena, uncontrolled proliferation and metastatic behavior, EMT, and chemoresistance. The common mediator of these actions appears to be exosomes that are released by vascular endothelial cells.

Exosomes are membrane-bound vesicles with nanometer dimensions. They are released from the plasma membrane of numerous cell types. Their membranes carry a variety of donor cell proteins, and their

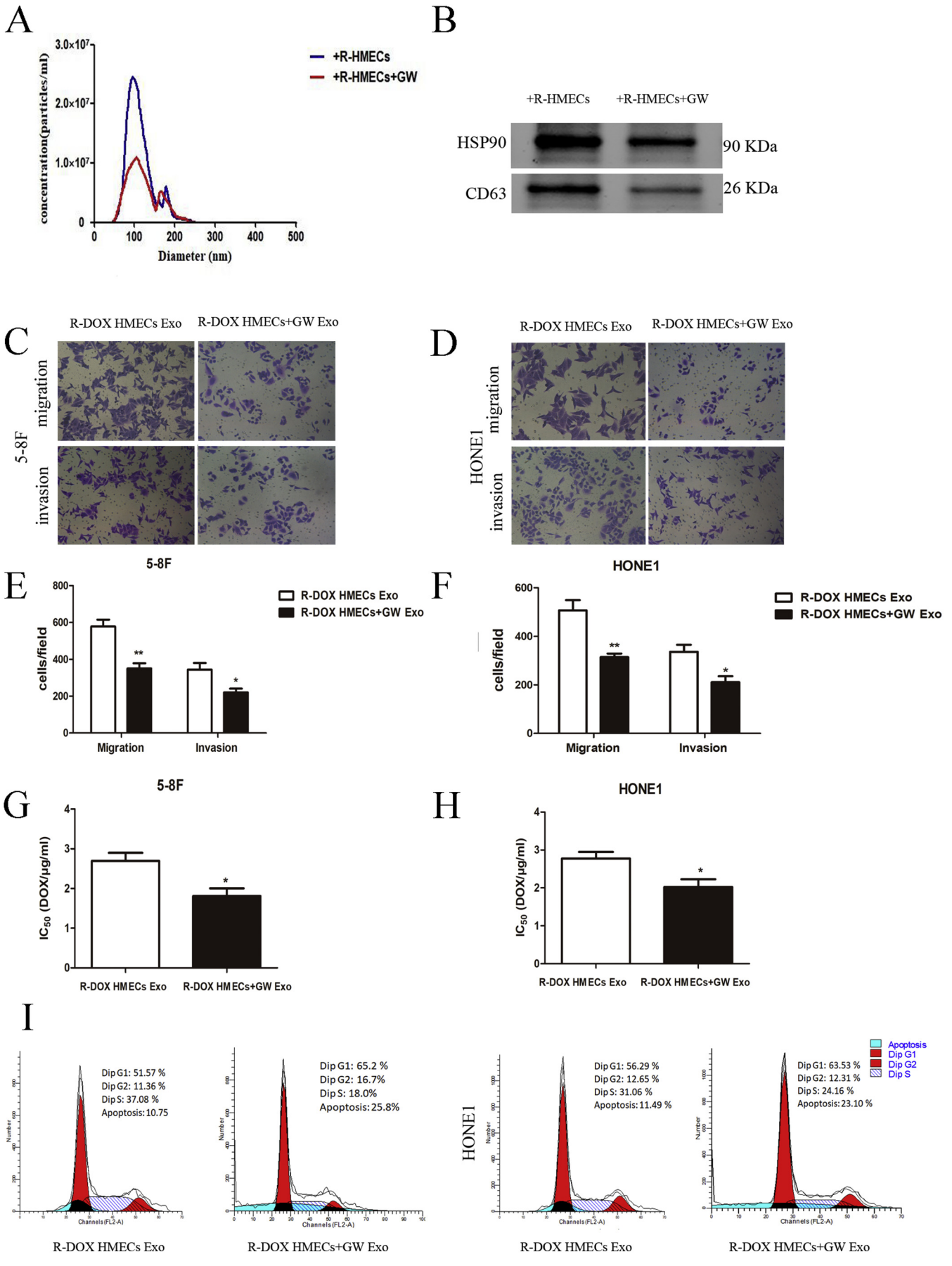

(caption on next page)

Fig. 3. R-DOX HMECs-derived exosomes promote NPC cell oncogenic phenotypes via derived exosomes. The size distribution of the isolated particles measured by NTA (A) and the detection of exosomal positive markers Hsp90 and CD63 in R-DOX HMEC-derived and N-DOX HMEC-derived exosomes by western blot analysis (B). The migration and invasion properties of 5-8F (C) and HONE1 (D) cells as determined by a Transwell assay and crystal violet staining. (E&F) Statistical results for (C& D). IC_{50} of 5-8F (G) and HONE1 (H) cells incubated with R-DOX HMEC-derived exosomes treated with or without GW4869 (the exosome inhibitor). (I) Effects of DOX on the 5-8F and HONE1 cell cycle distribution and the apoptosis rate. The cells were incubated with or without GW4869-treated HMEC-derived exosomes for 48 h. The data are presented as the means ± SEM of three independent experiments. * $P < .05$. (For interpretation of the references to colour in this figure legend, the reader is referred to the web version of this article.)

interiors have also been shown to carry various cytoplasmic contents. Exosomes have been shown in many systems to mediate intercellular communication, as appears to be the case in the model used in the present study [14].

Our findings are in accordance with those of Shi and colleagues [6], who studied the effects of exosomes generated by mesenchymal stem cells on NPC cells. The authors found that incubation of NPC cells with mesenchymal stem cells triggered EMT in the NPC cells, as well as proliferation and migration.

Cancer cells themselves have been shown to transmit chemoresistance from one cell to another via exosomes. Qin and coworkers [7] showed that lung cancer cells transferred resistance to cisplatin to other cancer cells via an exosome-mediated mechanism. The authors did not determine the precise factors responsible for cisplatin resistance.

Ji and colleagues [8] showed that exosomes derived from mesenchymal stem cells substantially increased the chemoresistance of gastric cancer cells both in vivo and in vitro. The mechanism of this transfer may have involved the CaM-Ks/Raf/MEK/ERK pathway, because inhibition of this pathway partially restored chemosensitivity.

Wang and colleagues [9] identified two-way exosomal communication between bone marrow stromal stem cells (BMSCs) and multiple myeloma (MM) cells. Exosomal transfer from BMSCs to MM cells enhanced proliferation and migration activities, as in the present study, as well as conferring resistance to the proteasome inhibitor bortezomib.

Deng and coworkers [15] detailed a complex mechanism in which lung cancer cells and myeloid-derived suppressor cells exchange exosomes that help confer a more aggressive phenotype to the cancer cells, including augmentation of resistance to doxorubicin. The mechanism appeared to involve exosomal transfer of microRNAs, that have been found to participate in exosomal intercellular communication in other systems, including regulation of inflammatory responses [16], communication between keratinocytes and melanocytes [17], and as vehicles for the delivery of therapies in stroke victims [18].

In the current study, we successfully established drug-resistant HMECs and demonstrated that these cells produced substantial amounts of exosomes of the expected size. HMECs conferred oncogenic phenotypes (proliferation, invasion, EMT, and drug resistance) in NPC cell lines and did so in an exosome-dependent manner. Finally, in a nude mouse xenograft model, we showed that drug-resistant HMECs promoted tumor growth, metastatic behavior, and drug resistance, also in an exosome-dependent manner.

In summary, our data suggest that vascular endothelial cells may promote the development of metastatic and drug-resistant behavior in nasopharyngeal cancer cells in an exosome-dependent manner. These findings add to the growing fund of knowledge regarding the targeting of exosomes and their contents in cancer therapeutics.

4. Materials and methods

4.1. Cell culture

Drug-resistant HMECs were obtained as described in our previous publication [19]. Briefly, HMECs were exposed to increasing doses of doxorubicin (DOX) from 0.001 μg/ml to 0.24 μg/ml over 12 weeks, and surviving cells were resistant to 0.24 mg/l DOX treatment. Human nasopharyngeal carcinoma cell lines 5-8F (highly-metastatic subclone) and HONE1 were purchased from the Shanghai Institute of Cell Biology, Chinese Academy of Sciences (Shanghai, China). Cells were maintained in Dulbecco's Modified Eagle's medium (DMEM, 11995065, Thermo Fisher Scientific, Rockford, IL, USA) medium with 10% heat-inactivated fetal bovine serum (FBS, 10099141; Invitrogen, Carlsbad, CA, USA) without exosomes (FBS was centrifuged at 200,000 ×*g* for 18 h to deplete exosomes) in a humidified chamber with 5% CO_2 at 37 °C.

4.2. RNA extraction and real time RT-PCR

Total RNA was extracted from exosomes and cells using Trizol reagent (Life Technologies, Carlsbad, CA, USA) and equal amounts of RNA were used for real time RT-PCR analyses. The cDNAs were synthesized using a reverse transcription kit according to the manufacturer's instructions (Vazyme, Nanjing, China). β-actin was used as an internal control. The sequences of the specific primers used are shown in Table 1.

4.3. Western blotting

Total protein was extracted from NPC cells using sample buffer (62.5 mmol/l Tris-HCl, pH 6.8, 2% SDS, 10% glycerol and 5% 2-β-mercaptoethanol) and protein concentrations were determined using the Pierce BCA Protein Assay Kit (Thermo Fisher Scientific). Total protein samples (30 μg) were separated using 9% polyacrylamide SDS gels and were transferred to polyvinylidene fluoride membranes (Millipore, Bedford, MA, USA). The membranes were incubated with rabbit polyclonal anti-TrpC5 antibody (1:1000; Abcam, Cambridge, UK; ab230216), anti-E-cadherin (1:500, Abcam, ab15148), rabbit monoclonal anti-MRP1 antibody (1:1000; Abcam, ab233383), anti-P-gp antibody (1:2000; Abcam, ab170904), anti-vimentin (1:500; Abcam, ab8978), anti-CD63 (1:1000, Santa Cruz Biotechnology, Santa Cruz, CA, USA; sc-365604), or anti-HSP90 (1:1000, Santa Cruz Biotechnology, sc-13119), followed by horseradish peroxidase-conjugated secondary antibody. An anti-β-actin antibody (1:1000; Sigma-Aldrich, St Louis, MO, USA; A2228) was used as a loading control. The protein bands were visualized with enhanced chemiluminescence (ECL) reagents and quantified using ImageJ software.

4.4. Exosome isolation and NanoSight tracking analysis

Exosomes were isolated by centrifugation using the ExoQuick-TC EV isolation kit (System Biosciences, Mountain View, CA, USA) according to the manufacturer's protocol. Briefly, cell supernatants collected from drug-resistant HMECs, non-resistant HMECs, and drug-resistant HMECs + GW4869 cultures in exosome-free conditioned media were concentrated using a Centriprep Centrifugal Filter 3 K Device (Millipore Corporation) and filtered through a 0.22-mm pore filter, followed by incubation with ExoQuick-TC exosome precipitation solution at 4 °C overnight. Exosomes were then harvested by centrifugation at 1500 ×*g* for 30 min and suspended in phosphate-buffered saline (PBS) or serum-free medium. The concentration of exosomal proteins was measured using a BCA protein assay kit (Thermo Fisher Scientific). Exosomes isolated as described above were characterized for particle size distribution and quantified on a NanoSight LM10 device (Nanosight, Amesbury, UK). The data were processed using Nanoparticle Tracking Analysis (NTA) 2.2 analytical software.

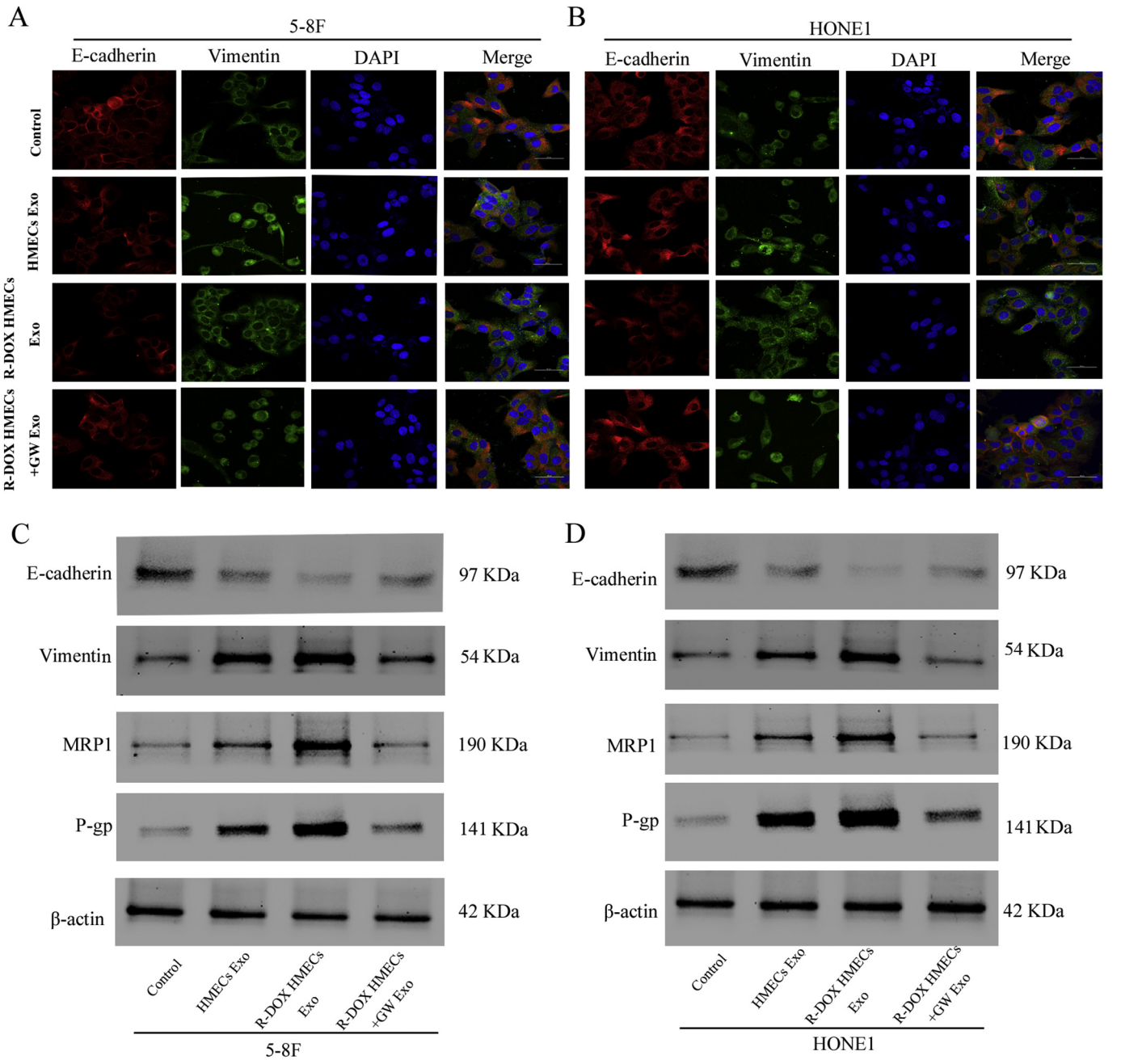

(caption on next page)

Fig. 4. EMT promoted in NPC cells by exosomes released from HMECs. Immunofluorescence assay was used to detect EMT-associated proteins in 5-8F (A) and HONE1 (B) cells incubated with exosomes derived from drug-resistant HMECs/DOX cells or non-drug-resistant HMECs/DOX cells treated with or without GW4869 (an exosome inhibitor). After staining, E-cadherin appears red, vimentin appears green, and nuclei stained with DAPI appear blue. The scale bar represents 50 μm. (C &D) The indicated cells were analyzed for the expression of EMT-related proteins by western blotting. The bar diagram (E&F) shows the relative expression of proteins normalized to β-actin. Data are represented as the means ± SEM of three independent experiments ($n = 3$, * $P < .05$; ** $P < .01$; *** $P < .001$; NS indicates not significant, $P > .05$). (For interpretation of the references to colour in this figure legend, the reader is referred to the web version of this article.)

4.5. Transmission electron microscopy

The resulting exosome pellets were fixed in 2% paraformaldehyde and adsorbed for 20 min to a Formvar carbon-coated grid. After adsorption, the samples were washed with PBS and transferred to a drop of 1% glutaraldehyde for 5 min. The grids were washed 8 times with Milli-Q water and negatively stained with 2% uranyl acetate for 5 min. The grids were then dried and visualized on a TECNAI 10 transmission electron microscope (Philips, Briarcliff Manor, NY, USA) at 80 kV. The images were captured using iTEM software (Olympus Soft Imaging Solutions, Center Valley, PA, USA).

4.6. Treatment with GW4869

GW4869 was used to block exosome formation and release. Drug-resistant HMECs were incubated in culture media with 10% exosome-free FBS containing 10 μM of GW4869 for 24 h to block exosome release.

4.7. Cell co-culture assay

Drug-resistant HMECs, non-resistant HMECs, or drug-resistant HMECs + GW4869 (5×10^5/well) were seeded into the upper chamber of a co-culture system and NPC cells (3×10^5/well) were placed in the lower chamber and incubated for 48 h. Co-cultured cells were separated using Transwell permeable supports (0.4 μm) in polycarbonate membrane 24-mm insert six-well plates (Costar, Cambridge, MA, USA).

4.8. Cell proliferation assay

The human nasopharyngeal carcinoma cell lines 5-8F or HONE1 (NPC cells) were seeded into 96-well plates at a concentration of 2000 cells/well in complete medium. At 24, 48, 72, and 96 h time points, cell proliferation assessment was carried out using the Cell Counting Kit-8 (CK04–20; Dojindo, Kumamoto, Japan), according to the manufacturer's protocol.

4.9. Cell migration and invasion assays

NPC cells (50,000 per well) were seeded into 24-well Transwell plates (Sigma-Aldrich) coated with or without Matrigel (BD Biosciences, San Jose, CA, USA). Cells were grown in DMEM containing 5 ng/ml TGF-β and were allowed to migrate and invade for 24 h. Photographs of five randomly selected fields of the fixed and crystal violet-stained cells were captured and cells that passed to the lower surface were counted. Experiments were repeated three times independently.

4.10. Immunofluorescence microscopy

Cells seeded onto coverslips in 24-well plates were subjected to immunochemical staining by incubation with primary anti-E-cadherin (1:50, Abcam, ab15148), or anti-vimentin antibodies (1:50; Abcam, ab8978) overnight, followed by AlexaFluor-conjugated secondary antibodies (Life Technologies, 1:1000) and nuclear staining with DAPI. Cells were observed by fluorescence microscopy.

4.11. Quantitative detection of apoptosis and cell cycle distribution

The cell cycle was analyzed using flow cytometry as previously described [20,21]. 5-8F and HONE1 cells (5.0×10^5 cells/well) were seeded in 6-well plates and grown until they reached 80% confluence. Then, the cells were treated with peimisine (15 μg/ml) for 24, 48, and 72 h. The cells were harvested, washed thrice with cold PBS, and fixed with 1.0 ml of 70% ethanol at 4 °C overnight. Then, cells were washed with PBS and incubated in 1.0 ml of PBS containing 100 μg propidium iodide and 100 μg RNase A in the dark for 30 min at 37 °C, and sorted in a FACScan flow cytometer using Kaluza 1.1 software (Beckman Coulter Inc., Fullerton, CA, USA).

4.12. Animal experiments

Male BALB/c nude mice (4–6 weeks old) were purchased from the Chinese Science Academy (Shanghai, China). All animal studies were conducted according to protocols approved by the Institutional Animal Care and Use Committee. Briefly, a combination of 2×10^6 5-8F cells and 1×10^6 drug-resistant HMECs were injected subcutaneously into the right axilla of each nude mouse to create the NPC model. All mice were intraperitoneally (IP) injected with GW4869 (1.25 mg/kg/day for 5 days before cell injection). When tumors became palpable (approximately 100 mm^3), mice were injected IP with GW4869 (1.25 mg/kg/day) and doxorubicin (2 mg/kg/day) ($n = 6$ per group) three times a week until day 27. Xenograft tumor size was monitored every three days (volume = $width^2 \times length \times 1/2$). Mice were euthanized at the end of the experiment and the tumors were excised. Tumors were fixed in 10% formalin, embedded in paraffin, and cut into 4-μm sections.

The lung metastasis model was created as previously described. The indicated NPCs and drug-resistant HMECs were resuspended in PBS and intravenously injected through the tail vein. Metastases were detected using the IVIS@ Lumina II system (Caliper Life Sciences, Hopkinton, MA, USA).

4.13. Immunohistochemistry

Sections of paraffin-embedded xenograft tissues were deparaffinized, rehydrated, subjected to microwave antigen retrieval in EDTA antigen retrieval buffer, incubated with 3% hydrogen peroxide, and non-specific binding was blocked using bovine serum albumin. The slides were incubated with anti-MRP1 (1:3000; Abcam, ab233383), anti-vimentin (1:100; Abcam, ab8978), or anti-Ki67 (1:200; Abcam, ab16667) primary antibodies, or were subjected to TUNEL staining. The staining processes were performed as previously described and quantified with Image ProPlus (IPP) software (Media Cybernetics, Rockville, MD, USA).

4.14. Statistical analysis

SPSS 16.0 software was used for statistical analysis. All results are presented as means ± SEMs. Differences between groups were analyzed using the two-tailed Student's *t*-test. P values < .05 were considered statistically significant.

Author contributions

Conceptualization, Limin Huang and Hui Chen; Data curation,

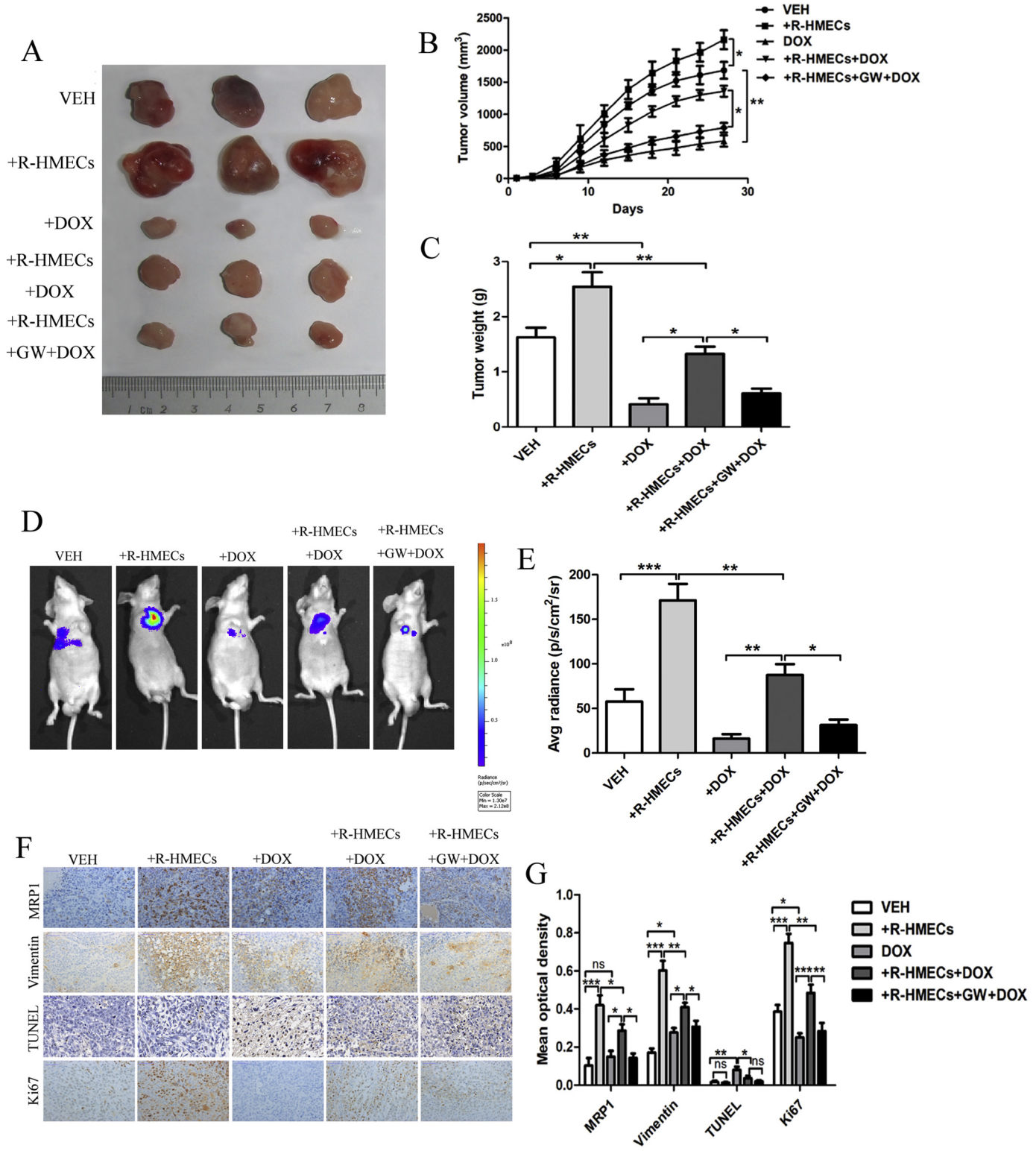

Fig. 5. Effect of drug-resistant HMECs on nude mice burdened with NPC xenografts mediated by exosomes. (A–C) Nude mice inoculated subcutaneously with 4×10^6 5-8F cells and 2×10^6 drug-resistant HMECs were treated with DOX (2 mg/kg/day), GW4869 (1.25 mg/kg/day), or both for 27 days. At the end of the treatment period, mice were euthanized and tumor specimens were harvested. The tumor volume was determined by measuring the length and width with calipers every 3 days (volume = width^2 × length × 1/2). The mean tumor volume for each treatment group is indicated. Results are represented as the means ± SEM of six mice per group ($n = 6$, * P < .05; ** P < .01). (D&E) Live imaging analysis was performed using the optical imaging system IVIS200. Representative images of intrahepatic metastasis foci are shown. Luciferase signal intensities of mice over time after tail vein injection with 2×10^6 indicated 5-8F cells and 1×10^6 HMECs/DOX cells were determined and the fluorescence signal in (D) was quantified ($n = 5$, ** P < .05; ** P < .01; *** P < .001). (F&G) Tumor specimens were subjected to immunohistochemical staining for MRP1, Vimentin, and Ki67, and cell apoptosis was examined by TUNEL staining. Images were captured at 400× magnification. The scale bar represents 50 μm. The mean density of each group (integrated optical density/area) is presented (n = 5, ** P < .05; ** P < .01; *** P < .001; NS indicates not significant, P > .05).

Table 1
Primer sequences used for real time RT-PCR analysis.

Gene name	Primer sequence (5′–3′)
TrpC5	Sense: GGGCTGAGACTGAGCTGTC Antisense: TTGCGGATGGCGTAGAGTAAT
MAP1	Sense: AAGGAGGTACTAGGTGGGCTT Antisense: CCAGTAGGACCCTTCGAGC
P-gp	Sense: TTGCTGCTTACATTCAGGTTTCA Antisense: AGCCTATCTCCTGTCGCATTA
β-actin	Sense: TCCGGCACTACCGAGTTATC Antisense: GATCCGGTGTAGCAGATCGC

Limin Huang and Chaoquan Hu; Formal analysis, Yong Li and He Lu; Investigation, He Lu; Methodology, Hui Chao; Project administration, Limin Huang, Chaoquan Hu, Hui Chao, Yu Zhang, jing Hou and Zhong Xu; Software, Chaoquan Hu, Yu Zhang and Yong Li; Writing – original draft, Limin Huang and Chaoquan Hu; Writing – review & editing, Hong Li and Hui Chen.

Declaration of Competing Interest

None.

Acknowledgments

This study was supported by the National Natural Science Foundation of China (No. 81660451); The Science and Technology Department of Guizhou Province (No. 20157171).

References

[1] K.O. Lam, A.W. Lee, W.T. Ng, K.I. Hopkins, The International Atomic Energy Agency global initiatives on nasopharyngeal cancer treatment, Chin. Clin. Oncol. 5 (2) (2016) 27.
[2] C.S. Ho, Beating 'Guangdong cancer': a review and update on nasopharyngeal cancer, Hong Kong Med. J. = Xianggang Yi Xue Za Zhi 23 (5) (2017) 497–502.
[3] S.C. Liu, C.M. Huang, O.A. Bamodu, C.S. Lin, B.L. Liu, Y.M. Tzeng, J.T. Tsai, W.H. Lee, T.M. Chen, Ovatodiolide suppresses nasopharyngeal cancer by targeting stem cell-like population, inducing apoptosis, inhibiting EMT and dysregulating JAK/STAT signaling pathway, Phytomedicine 56 (2019) 269–278.
[4] P. Blanchard, A. Lee, S. Marguet, J. Leclercq, W.T. Ng, J. Ma, A.T. Chan, P.Y. Huang, E. Benhamou, G. Zhu, D.T. Chua, Y. Chen, H.Q. Mai, D.L. Kwong, S.L. Cheah, J. Moon, Y. Tung, K.H. Chi, G. Fountzilas, L. Zhang, E.P. Hui, T.X. Lu, J. Bourhis, J.P. Pignon, M.-N.C. Group, Chemotherapy and radiotherapy in nasopharyngeal carcinoma: an update of the MAC-NPC meta-analysis, Lancet Oncol. 16 (6) (2015) 645–655.
[5] W.L. Tay, G.W. Yip, P.H. Tan, K. Matsumoto, R. Yeo, T.P. Ng, S.D. Kumar, M. Tsujimoto, B.H. Bay, Y-Box-binding protein-1 is a promising predictive marker of radioresistance and chemoradioresistance in nasopharyngeal cancer, Modern Pathol. 22 (2) (2009) 282–290.
[6] S. Shi, Q. Zhang, Y. Xia, B. You, Y. Shan, L. Bao, L. Li, Y. You, Z. Gu, Mesenchymal stem cell-derived exosomes facilitate nasopharyngeal carcinoma progression, Am. J. Cancer Res. 6 (2) (2016) 459–472.
[7] X. Qin, S. Yu, L. Zhou, M. Shi, Y. Hu, X. Xu, B. Shen, S. Liu, D. Yan, J. Feng, Cisplatin-resistant lung cancer cell-derived exosomes increase cisplatin resistance of recipient cells in exosomal miR-100-5p-dependent manner, Int. J. Nanomedicine 12 (2017) 3721–3733.
[8] R. Ji, B. Zhang, X. Zhang, J. Xue, X. Yuan, Y. Yan, M. Wang, W. Zhu, H. Qian, W. Xu, Exosomes derived from human mesenchymal stem cells confer drug resistance in gastric cancer, Cell Cycle 14 (15) (2015) 2473–2483.
[9] J. Wang, A. Hendrix, S. Hernot, M. Lemaire, E. De Bruyne, E. Van Valckenborgh, T. Lahoutte, O. De Wever, K. Vanderkerken, E. Menu, Bone marrow stromal cell-derived exosomes as communicators in drug resistance in multiple myeloma cells, Blood 124 (4) (2014) 555–566.
[10] R.J. Lobb, R. van Amerongen, A. Wiegmans, S. Ham, J.E. Larsen, A. Moller, Exosomes derived from mesenchymal non-small cell lung cancer cells promote chemoresistance, Int. J. Cancer 141 (3) (2017) 614–620.
[11] K.B. Challagundla, P.M. Wise, P. Neviani, H. Chava, M. Murtadha, T. Xu, R. Kennedy, C. Ivan, X. Zhang, I. Vannini, F. Fanini, D. Amadori, G.A. Calin, M. Hadjidaniel, H. Shimada, A. Jong, R.C. Seeger, S. Asgharzadeh, A. Goldkorn, M. Fabbri, Exosome-mediated transfer of microRNAs within the tumor microenvironment and neuroblastoma resistance to chemotherapy, J. Natl. Cancer Inst. 107 (7) (2015).
[12] D.S. Wong, D.G. Jay, Emerging roles of extracellular hsp90 in cancer, Adv. Cancer Res. 129 (2016) 141.
[13] A. Sparreboom, J. Verweij, Advances in cancer therapeutics, Clin. Pharmacol. Ther. 85 (2) (2009) 113–117.
[14] A.V. Vlassov, S. Magdaleno, R. Setterquist, R. Conrad, Exosomes: current knowledge of their composition, biological functions, and diagnostic and therapeutic potentials, Biochim. Biophys. Acta 1820 (7) (2012) 940–948.
[15] Z. Deng, Y. Rong, Y. Teng, X. Zhuang, A. Samykutty, J. Mu, L. Zhang, P. Cao, J. Yan, D. Miller, H.G. Zhang, Exosomes miR-126a released from MDSC induced by DOX treatment promotes lung metastasis, Oncogene 36 (5) (2017) 639–651.
[16] D. Xu, M. Song, C. Chai, J. Wang, C. Jin, X. Wang, M. Cheng, S. Yan, Exosome-encapsulated miR-6089 regulates inflammatory response via targeting TLR4, J. Cell. Physiol. 234 (2) (2019) 1502–1511.
[17] Y. Liu, L. Xue, H. Gao, L. Chang, X. Yu, Z. Zhu, X. He, J. Geng, Y. Dong, H. Li, L. Zhang, H. Wang, Exosomal miRNA derived from keratinocytes regulates pigmentation in melanocytes, J. Dermatol. Sci. 93 (3) (2019) 159–167.
[18] Z.G. Zhang, B. Buller, M. Chopp, Exosomes - beyond stem cells for restorative therapy in stroke and neurological injury, Nat. Rev. Neurol. 15 (4) (2019) 193–203.
[19] L. Huang, C. Perrault, J. Coelho-Martins, C. Hu, C. Dulong, M. Varna, J. Liu, J. Jin, C. Soria, L. Cazin, A. Janin, H. Li, R. Varin, H. Lu, Induction of acquired drug resistance in endothelial cells and its involvement in anticancer therapy, J. Hematol. Oncol. 6 (1) (2013) 49.
[20] D.Z. Wang, J.F. Gao, S.F. Jing, H. Wei, X.Y. Huang, C.D. Li, Antitumor effect of Docetaxel in osteosarcoma by the inhibition of Wnt signal channel, Drug Res. 65 (11) (2015) 597–601.
[21] Y.S. Ma, S.W. Weng, M.W. Lin, C.C. Lu, J.H. Chiang, J.S. Yang, K.C. Lai, J.P. Lin, N.Y. Tang, J.G. Lin, J.G. Chung, Antitumor effects of emodin on LS1034 human colon cancer cells in vitro and in vivo: roles of apoptotic cell death and LS1034 tumor xenografts model, Food Chem. Toxicol. 50 (5) (2012) 1271–1278.